Mon. Not. R. Astron. Soc. **000**, 000–000 (0000) Printed 4 April 2014 (MN LATEX style file v2.2)

The secular evolution of the Kuiper belt after a close stellar encounter

D. Punzo[1 2], R. Capuzzo-Dolcetta[1], S. Portegies Zwart[3]
[1] *Dep. of Physics, Sapienza, University of Roma, P.le A. Moro 1, Roma, Italy*
[2] *Kapteyn Institute, Rijksuniversiteit, Landleven 12, 9747AD Groningen, Netherlands*
[3] *Leiden Observatory, Leiden University, P.O. Box 9513, 2300 RA Leiden, The Netherlands*

arXiv:1403.6633v2 [astro-ph.EP] 3 Apr 2014

4 April 2014

ABSTRACT

We show the effects of the perturbation caused by a passing by star on the Kuiper belt objects (KBOs) of our Solar System. The Kuiper belt is sampled using up to 131,072 bodies on nearly circular orbits distributed in a ring of surface density $\Sigma \sim r^{-2}$. The dynamics of the KB is followed by direct N- body simulations. The growth of a dynamically hot population as well as the population in resonance orbits with the planets, depends on the distribution of individual masses of Kuiper belt objects, the total mass and its radial extent, as well as on the mass and the orbit of the passing by star. The Kuiper belt is rather fragile for an encounter with a passing star, and the cross section threshold above which a recognizable structure is left are quite small. We chose for the encountering star a mass $0.5\,M_\odot$ to $2\,M_\odot$ with an impact parameter of 170 AU (for a $0.5\,M_\odot$ star) to 220 AU (for $2\,M_\odot$) and an inclination angle (θ) of 60° (for $0.5\,M_\odot$) to 120° (for $2\,M_\odot$). This results in a post encounter distribution which compares best to the currently observed population. These encounters, however, tend to excite the cold population ($e \lesssim 0.1$ around $a \sim 40$ AU), and consequently depletes this area. Subsequent secular evolution of the Kuiper belt can repopulate this area in less than 1 Myr if at least $\gtrsim 35\%$ of the KBOs are relatively massive ($m \sim M_{Pluto}$). However, we did not consider the effect of the secular evolution of a larger population of somewhat less massive objects over a longer time scale, which may result in a similar repopulation of the cold Kuiper belt. We therefore speculate that the early Kuiper belt contained a rich ($\gtrsim 35\%$) population of objects with mass $\sim M_{\rm Pluto}$.

Key words: Kuiper belt objects; Solar System Dynamics; methods: numerical.

1 INTRODUCTION

The Solar System is hedged by a ring composed of a huge number of small bodies: the Edgeworth-Kuiper belt (Jewitt & Luu 1993) (hereafter briefly called Kuiper belt, or KB). The Kuiper belt bears the signature it the early evolution of the Solar System, and a contains records of the end-state of the accretion processes occurred in that region. Therefore, the knowledge of the history of the Kuiper belt objects (KBOs) is relevant to be able to develop a full consensus of the formation of the Solar System.

from the Sun, but most are around the 2:3 resonance with Jupiter, at 39.5 AU and at its 1:2 resonance, roughly around 48 AU. The total mass is estimated from 0.01 to 0.1 $M_\oplus$ (Luu & Jewitt 2002). There are several, indirect, arguments suggesting that this is just a small fraction of its initial mass because most of it has been lost (see Kenyon & Luu (1999)). The size distribution of the KBOs is, usually, assumed as a power law $dn/dR = AR^{-q}$, where A and q are constants. The q exponent is estimated $\sim 4.0\pm0.5$ (Bernstein et al. 2004; Fraser & Kavelaars 2009). For a more detailed description of the Kuiper belt we refer, e.g., to Luu & Jewitt (2002).

The KB consists of two separate populations (Brown 2001). The *dynamically cold* population refers to objects on nearly circular orbits, i.e. with orbital eccentricities less than 0.1, and moving on a plane with relatively low inclinations (up to about 10°) respect to the ecliptic. On the other side, the dynamically hot population is characterized highly inclined orbits (up to 40°) with respect to the ecliptic and eccentricities $\gtrsim 0.1$.

In Fig. 1 the eccentricities and inclinations are plotted as function of the semi-major axis for KBOs observed from the Minor Planet Center (MPC) (Marsden 1980) which is the center of the Smithsonian Astrophysical Observatory

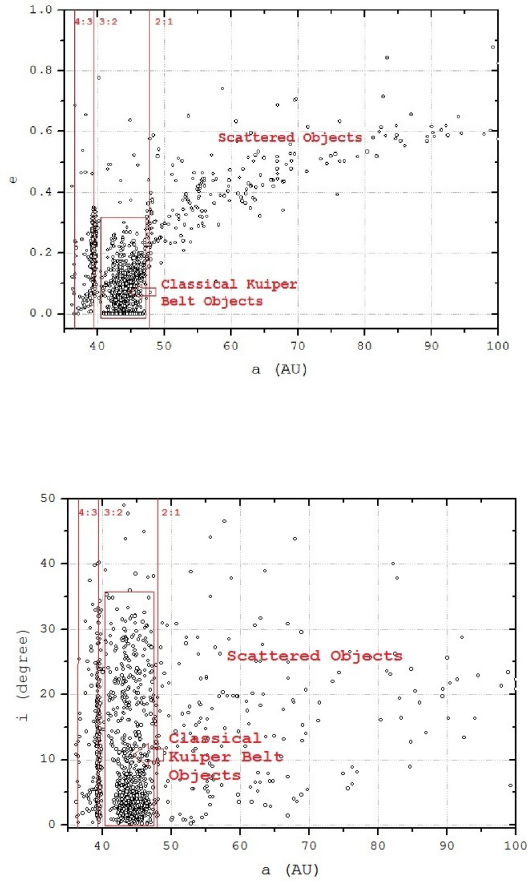


Figure 1. distribution of the eccentricities (top panel) and inclinations (bottom panel) as a function of semi-major axis of the observed KBOs; data are from the Minor Planet Center (Marsden 1980). The vertical lines highlight the main resonances.

(SAO) dedicated to tracking, monitoring, calculating and disseminating data from asteroids and comets.

Te KBOs have been sub-categorized in three groups:

(i) classical KBOs ($42 < a < 49$, $\langle e\rangle \simeq 0.09$, $\langle i\rangle \simeq 7^\circ$);
(ii) scattered KBOs ($a > 30$, $\langle e\rangle \simeq 0.49$, $\langle i\rangle \simeq 14^\circ$);
(iii) main resonant KBOs :

- 4:3 resonance ($a \simeq 36,4$, $\langle e\rangle \simeq 0.22$, $\langle i\rangle \simeq 8^\circ$);
- 3:2 resonance, Plutino's ($a \simeq 39.4$, $\langle e\rangle \simeq 0.36$,$\langle i\rangle \simeq 13^\circ$);
- 2:1 resonance ($a \simeq 47.8$, $\langle e\rangle \simeq 0.14$, $\langle i\rangle \simeq 10^\circ$).,

where semimajor axes, a, are in AU.

These sub-populations have been explain through a phase of planet migration and a phase of clearing of the environment during the evolution of the early Solar System (Malhotra 1993, 1995). In the latter phase the resonance population was formed by sweeping resonance capture in which the Jovian planets withstand considerable orbital migration as a result of encounters with residual planetesimals. While Neptune moved outwards, a small body like Pluto in an initially circular orbit could have been captured into the 3:2 resonance. The high orbital eccentricity would subsequently be induced by repeated orbital crossings with Neptune.

Many others studies have attempted to better understand the properties of the KBOs. Gomes (2003) investigated how the outward migration of Neptune, as proposed by (Malhotra 1993, 1995), could have scattered objects from 25 *AU* onto high-i orbits leading to the current classical Kuiper belt region. He concluded that the high-i population was formed closer to the Sun and brought into the classical Kuiper belt during planetary migration, whereas the cold population represents a primordial, relatively undisturbed population. This also led to the speculation that other mechanisms, such as planetary migration, have been the cause of the correlation between inclinations and colors in the classical Kuiper belt rather than environmental effects like the collisions among the KBOs (see Doressoundiram et al. (2008)). Detailed discussions about the correlation of the inclination with the color, size and binary of the KBOs are given by Levison & Stern (2001); Brucker et al. (2009); Noll et al. (2008); Volk & Malhotra (2011). More recently a model, called the Nice model, has been proposed (Levison et al. 2008), which argues that the giant planets migrated from an initial compact configuration into their present orbits, long after the dissipation of the initial protoplanetary gas disk. The Nice model seems to provide a acceptable explanation for the formation of the classical and scattered populations, and for the correlation between inclinations and colors (for more detail see Levison et al. (2008)). The Nice model, however, predicts a higher eccentricities in classical KBO orbits than is observed.

An interaction between a passing field star and the the Solar System could also be responsible for some of the orbital families observed in the KBO, which is the main topic of this paper.

2 THE FLY-BY STAR PERTURBATION AND THE N-BODY SCHEME

An encounter between a passing star and the Solar System is quite likely, considering that the Solar System was probably formed in an open star cluster (Portegies Zwart 2009). The hypothesis of a closely passing star has been hypothesized before, and used to explain KBO families (Ida et al. 2000; Kobayashi & Ida 2001; Kobayashi et al. 2005; Melita et al. 2005; Malmberg et al. 2011). The cost of such calculations, however, has dramatically limited the covered parameter-space and prevented earlier research on the secular evolution of the KBO.

We investigate the effects of a close stellar encounter on the structure of the Kuiper belt, and its subsequent long-term evolution. We adopt a direct N-body treatment in which the pair-wise interactions between KBOs, planets and stars are taken into account self-consistently. Due to the computational expense of this method we are limited to about $N \leqslant 131,072$.

We modeled the early Solar System as composed by the Sun, the eight major planets, Pluto and the Kuiper belt. Each object was considered a point-mass; we did not account for collisions. The KBOs were initially moving in circular orbits in a flat ring in the plane of the ecliptic. This corresponds to an initially cold population, without a

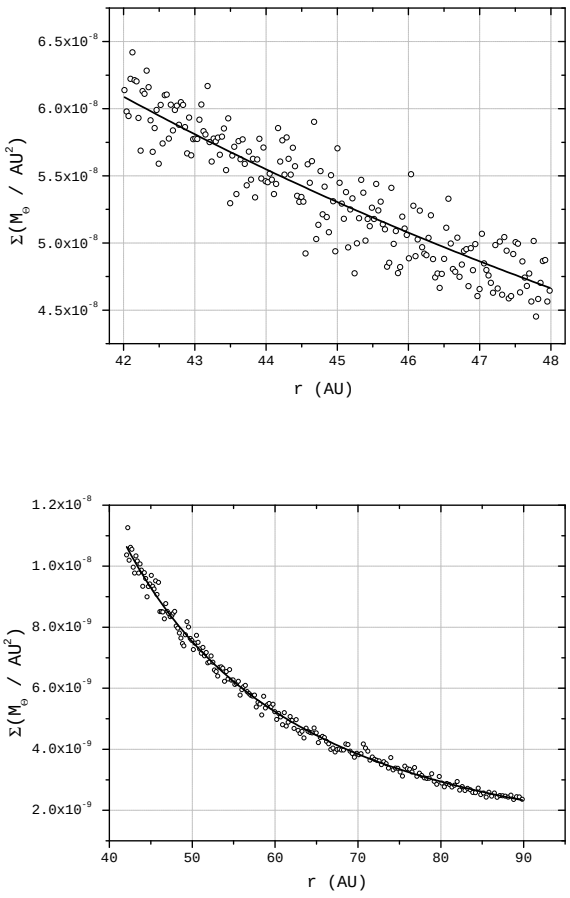


Figure 2. The initial surface density Σ of model A, with $M = 30 M_\oplus$ (top panel) and for model B (bottom panel).

$z-$component in their motion. We adopted a surface density $\Sigma \propto r^{-2}$, where r is the heliocentric distance (see Holman (1995)).

We studied two possible configurations:

- (i) model A, with a radial extension in the range from 42 *AU* to 48 *AU* and four different values of the total mass of the KB, $M = 3, 6, 1, ; 30$ M$_\oplus$;
- (ii) model B, with a radial extension in the range from 42 *AU* to 90 *AU* and a total mass $M = 30\ M_\oplus$.

The mass function of the KBOs was derived from the conversion in mass of the size (R) distribution, assuming a constant KBO density (i.e. $\rho \sim 10^3$ kg/m^{-3}), which results in $dm/dR \propto R^{-2.0\pm0.5}$ with a cut at $m_{min} \approx 6.7\ 10^{-13} M_\oplus$ (corresponding to $R = 1$ km) and $m_{max} \approx 1.7\ 10^{-3} M_\oplus$ (corresponding to $R = 10^3$ Km). In Fig. 2 we present the surface density of the models A and B as a function of the heliocentric distance for KBOs with the same individual mass, $m = M/N$. Here M is the total mass of the Kuiper belt and N the number of KBOs. With this choice we have a good sampling of the KB without an exceedingly large number ($N > 10^6$) of particles.

We integrate the equations of motion by direct summation N-body codes running on Graphics Processing Units (GPUs). For the gravitational N-body problem these accelerators give a manifold speed increase with respect to code running on CPU Nyland et al. (2007); Portegies Zwart et al. (2007); Bédorf & Portegies Zwart (2012). Parallel computers equipped more than one hundred GPUs have been utilized for various studies Capuzzo-Dolcetta et al. (2013); Capuzzo-Dolcetta & Spera (2013); Berczik et al. (2011, 2013) have been run efficiently in parallel to provide the computational power necessary to perform direct many body simulations. Access to such large GPU-equipped supercomputers, however, is not easy, in particular when the computations required a considerable fraction of the available hardware. We therefore mainly ran our simulation on the Little Green Machine, a at the Sterrewacht Leiden built dedicated GPU-equipped supercomputer, specifically built for performing GPU-related calculations. Even with this machine, we had to limit the number of bodies to about a hundred thousand, but we performed several simulations (of models A and B) for each realization of the initial conditions in order to assure that the results of our calculations were not a statistical anomaly. Recently Portegies Zwart & Boekholt (2014) demonstrated that performing multiple simulations with the same initial conditions provide a statistically correct sampling of the real solutions. In these runs we varied the mass, impact parameter and the inclination of the incoming star.

$$\begin{cases} M_\star = [0.5; 1; 2] \mathrm{M}_\odot & \\ \quad x = 500 & v_{x,\infty} \simeq -3, \\ \quad y = b\cos\theta & v_{y,\infty} = 0, \\ \quad z = b\sin\theta & v_{z,\infty} = 0, \end{cases} \tag{1}$$

where x, y, z are in AU and velocities in km/s. The system of reference was centered on the Sun, and the impact parameters b and inclination θ characterize the orbit of the encountering star. The incoming star was placed in a ring of radius b at a distance of 500 AU in the x-direction parallel to the yz plane. In Tab. 1 we present the initial conditions for our simulations.

Calculations were performed using the direct summation code `HiGPUs` (Capuzzo-Dolcetta et al. 2013), which is publicly available via the Astronomical Multipurpose Software Environment (AMUSE) (Portegies Zwart et al. 2009; Pelupessy et al. 2013; Portegies Zwart et al. 2013).

This code uses its own kernels to implement at best a 6th-order Hermite's integrator (Nitadori & Makino 2008) with block time-steps (Aarseth 2003) method.

We tested the accuracy of `HiGPUs` with the two symplectic N-body codes, `HUAYNO` (Pelupessy et al. 2012), which uses recursive-Hamiltonian splitting to generate multiple-timestep integrators that conserve momentum to machine precision, and `NBSymple` (Capuzzo-Dolcetta et al. 2011), which is based on a symplectic second and sixth order method for the time integration of the equations of motion. The comparison indicates as fully reliable the simulations done with the fast `HiGPUs` code.

All the simulations were performed using a softening parameter, ϵ, in the pairwise Newtonian potential $U_{ij} \propto \sqrt{r_{ij}^2 + \epsilon^2}$, where r_{ij} is the $i-th$ to $j-th$ particle distance. Note that the ϵ value was set to 4×10^{-4} *AU*, which was

index	b	θ	$y(AU)$	$z(AU)$	index	b	θ	$y(AU)$	$z(AU)$
1	140	90	0.000	140.000	33	200	30	173.205	100.000
2	140	100	-24.311	137.873	34	200	60	100.000	173.205
3	140	110	-47.883	131.557	35	200	70	68.404	187.939
4	150	30	129.904	75.000	36	200	75	51.764	193.185
5	150	60	75.000	129.904	37	200	80	34.730	196.962
6	150	90	0.000	150.000	38	200	90	0.000	200.000
7	150	100	-26.047	147.721	39	200	105	-51.764	193.185
8	150	110	-51.303	140.954	40	200	120	-100.000	173.205
9	150	120	-75.000	129.904	41	200	135	-141.421	141.421
10	150	150	-129.904	75.000	42	200	150	-173.205	100.000
11	160	90	0.000	160.000	43	212.5	60	106.250	184.030
12	160	100	-27.784	157.569	44	212.5	75	54.999	205.259
13	160	110	-54.723	150.351	45	212.5	90	0.000	212.500
14	170	90	0.000	170.000	46	212.5	105	-54.999	205.259
15	170	100	-29.520	167.417	47	212.5	120	-106.250	184.030
16	170	110	-58.143	159.748	48	212.5	135	-150.260	150.260
17	170	90	0.000	170.000	49	212.5	150	-184.030	106.250
18	170	100	-29.520	167.417	50	225	30	194.856	112.500
19	170	110	-58.143	159.748	51	225	60	112.500	194.856
20	175	30	151.554	87.500	52	225	75	58.234	217.333
21	175	60	87.500	151.554	53	225	90	0.000	225.000
22	175	70	59.854	164.446	54	225	105	-58.234	217.333
23	175	80	30.388	172.341	55	225	120	-112.500	194.856
24	175	90	0.000	175.000	56	225	135	-159.099	159.099
25	175	120	-87.500	151.554	57	225	150	-194.856	112.500
26	175	150	-151.554	87.500	58	237.5	60	118.750	205.681
27	180	70	61.564	169.145	59	237.5	75	61.470	229.407
28	180	80	31.257	177.265	60	237.5	90	0.000	237.500
29	180	90	0.000	180.000	61	237.5	105	-61.470	229.407
30	190	70	64.984	178.542	62	237.5	120	-118.750	205.681
31	190	80	32.993	187.113	63	237.5	135	-167.938	167.938
32	190	90	0.000	190.000	64	237.5	150	-205.681	118.750

Table 1. The initial impact parameter b and inclination θ, and position in y and z of the incoming star for each of the 64 simulations performed. The system of reference is centered at the Sun.

$\sim$ 8 times smaller than the initial closest neighbour inter particle distance. The maximum time step for the hierarchical block time steps was $\sim 0.02\ yr$. The energy conservation was checked along the system evolution by its fractional time variation defined as

$$\frac{|\Delta E}{E}| = \left|\frac{E(t) - E(0)}{E(0)}\right|. \quad (2)$$

At the end of the simulations it was always below the value 10^{-7}, which is more than sufficient to assure that we statistically correctly sample the result of a true (converged) solution to the N-body problem (Portegies Zwart & Boekholt 2014).

3 RESULTS

Here we report on the results of the simulations using our two initial conditions, model A and model B.

3.1 Model A

In model A we adopted a radial extension of the KBO between 42 AU to 48 AU using a total mass of $M = 1$, 3, 6 and 30 $M_\oplus$. The mass and encounter parameters of the incoming star are presented in Tab. 1. The simulations are carried out until the perturbation induced by the passing star is negligible, even compared to the inter KBO forces (the gravitational contribute on the total force on a generic KBO due the passing star is five magnitude lower respect the Sun and one magnitude comparing with the nearest KBO neighbor).

In Fig. 3 we give the distribution of the KB as obtained by model A. The figure presents the projection of the sampled system onto the xy and the yz planes ~ 2500 yr after the closest approach between the Sun and the perturbing star. Some KBOs were scattered out to a heliocentric distances exceeding 200 AU, and with very high eccentricities, but the majority ($\sim 73\%$) of objects remains bound. Moreover the KBOs are distributed in over densities triggered by the passing of the star which are resonances due to the planets contribution.

In Figs. 4 and 5 we show the distributions for eccentricity and inclination as a function of the semi-major axis for the KBOs from model A. Here we varied the impact parameter parameters b and inclination θ of the encounter. The mass of the passing-by star was 1 $M_\odot$ for these simulations and the total mass of the KB was 30 $M_\oplus$. These simulations were performed with $N = 8192$ KBOs and run up to 10^4 yr.

In the Figures we have identified three main regimes, which we colored red, green and blue, indicating the highly, intermediate and relatively little perturbed system, respectively.

In the highly perturbing encounter (red zone in figs. 4

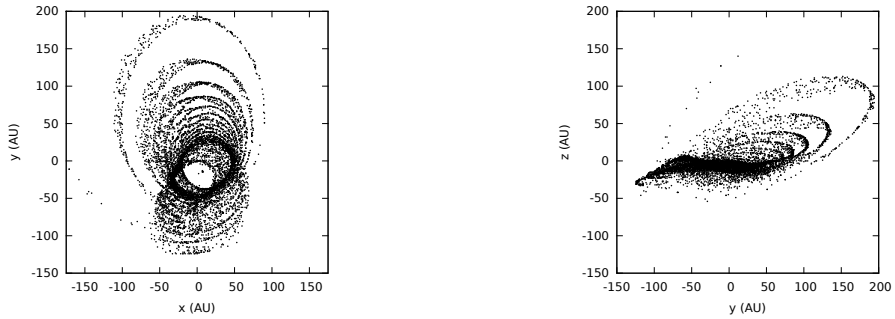


Figure 3. distribuion of the $N = 8192$ Kuiper belt objects in the xy plane (left panel) and in the yz plane (right panel) after an encounter with a $1\,M_\odot$ star (at $T = 3.2 \times 10^3$ yr) with parameters $b = 175$ AU and $\theta = 90°$.

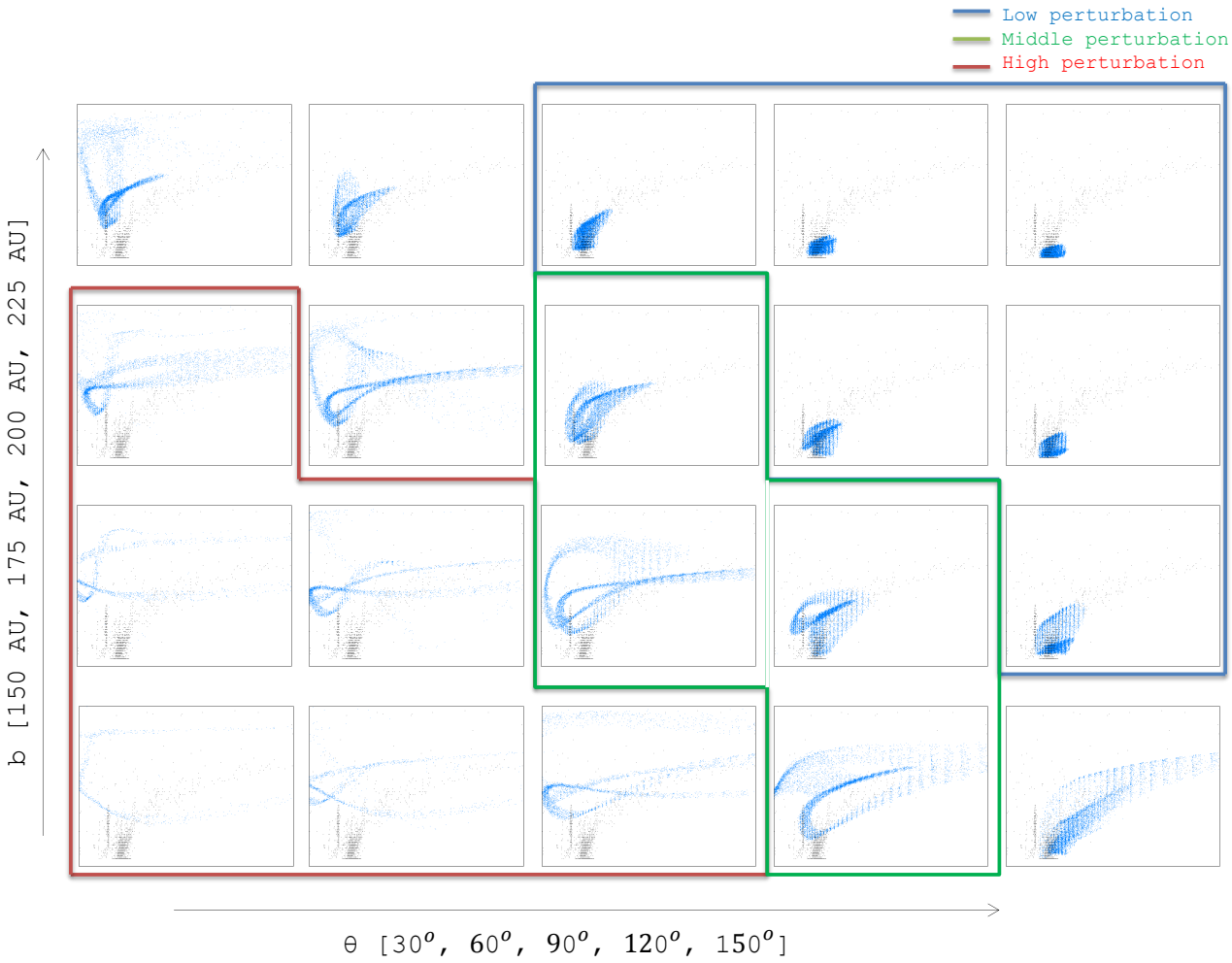


Figure 4. Parameter coverage of the eccentricities (betweeon 0 and 1) as a function of the semi-major axis (betwen 35 AU and 100 AU) for model A at 10^4, yr after the encounter. For readability we omitted the axis tickmarks and numbers, but each panel has identical axes as the images presented in the top panel of Fig. 1. The mass of the passing-by star was $1\,M_\odot$ and the total mass of the Kuiper belt was assumed equal to $30M_\oplus$. The black dots give the observed data from the MPC (Marsden 1980) (see also Fig. 1) and the blue dots give the simulated data. Each plot has different values of parameters b and θ ordered in increasing values. We identified three regimes in which the interaction had a strong influence on the distribution of KBOs (red), moderate (green) and mild (blue).

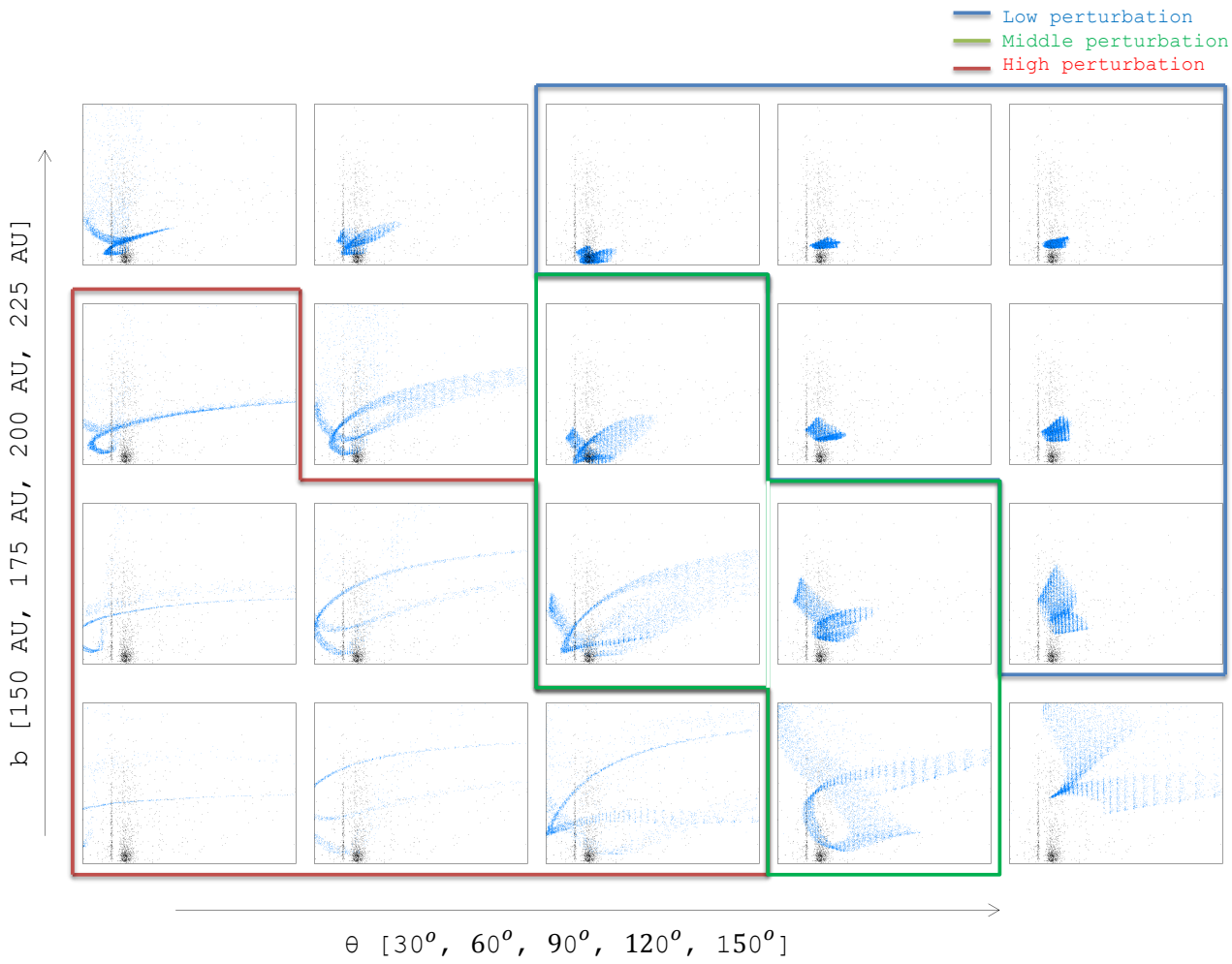


Figure 5. As fig. 4 but then for the inclination (between 0 and 50°).

and 5) the KB is almost completely destroyed. In the moderately perturbing encounter (blue zone) the post-encounter KBO is characterized by that the majority of objects remain confined in the classical region but with slightly elevated eccentricities and inclinations. These distributions are most comparable to the observed eccentricities and inclinations in the classic (observed) regions. However, the resonance regions and the scattered region are notoriously depleted compared to the observations. In particular, the distribution in inclinations is too much concentrated around a mean value, whereas the observed inclinations are distributed more evenly between 0° to 40°.

The distribution of eccentricities in the mildly perturbed encounters (green zone in figs. 4 and 5) has almost vanished and some objects have scattered to very small semi-major axes. The general shape of the KBO, however, seems to follow the data more closely that those that result from the other more strongly perturbed interactions. The majority of bodies resides in the classical part of the KB with an extended tail of monotonically increasing eccentricities with the semi-major axis, indicating an almost constant periastron distance. On the down-side, however, the distribution of inclinations is distinctively different than the observations.

We compare the distributions in eccentricities and inclinations of the KBOs at 10^4 yr after the encounter changing the total mass of the KB with values $1, 3, 6$ and $30\,M_\oplus$ and the sampling of the KBOs with N in range [8192, 131,072] fixing the $b = 200\,AU$ and $\theta = 90°$ parameters. This comparison is performed using the two-dimensional Kolmogorv-Smirnov tests (Press et al. 2002). The tests give probabilities for eccentricity as well as inclination $\geqslant 91.2\%$. The K-S test is a measure of the difference in the two distributions. The high values of these K-S test is an indication that the distributions, obtained varying the principal parameters of the sampling of the KB, show very small differences. Therefore, a small variation of the initial conditions for the KB gives rise to only small changes in final distribution, and on the short time frame of the encounter, the effect of the passing star is considerably stronger than any internal dynamical effect inside the KB. The effect the passing star has on the KB is almost impulsive, and variations in the mass of the passing star strongly affects the eccentricities and inclinations of the KBOs. These distributions therefore provide a sensitive characterization to constrain the mass and orbital parameters of the incoming star. But we probably could as well have simulation the encounter with a restricted few-body approach, neglecting the internal interactions between the KBOs.

The strong effect of the incoming star is clearly depicted in Figs. 4 and 5. Varying the mass of the encountering star cases a migration in both b and θ. The low-mass star ($0.5\,M_\odot$) gives rise to a shift to smaller values of b and θ, whereas a higher mass star ($2\,M_\odot$) causes a shift toward larger values of both parameters.

The early evolution of the system strongly depends on the initial conditions of the passing star. We therefore decided to run more simulations in the middle regime (green zone) in the range $\theta = [70, 80, 90]^\circ$ and $b = [170, 180, 190, 200]$ UA, and in a the second regime of $\theta = [90, 100, 110, 120]^\circ$ and $b = [140, 150, 160, 170]$ AU. All the simulations show a characteristic tail to a monotonically increasing eccentricities; quite similar to the distribution of the eccentricities of the observed scattered KBOs. This tail is characteristic for the relatively close encounter with a stellar perturber, and we confirm the earlier made conjecture of such an encounter (Ida et al. 2000). The distribution in inclination, however, is still to easily reproduced.

To validate our visual comparison we performed a statistical cross-comparison between the observational and computational data for each of the simulations in Tab. 1 using the Hotelling's two sample T^2 test (Hotelling 1931), which is a generalization of the Student's t test, where

$$T^2 = \frac{(n_1 + n_2 - 2)p}{n_1 + n_2 - p - 1} F, \tag{3}$$

with F the Fisher-Snededecor random variable. The Hotelling's test states that two population are indistinguishable if

$$F \lesssim F_{tab}(p, n_1 + n_2 - 1 - p), \tag{4}$$

where n_1 and n_2 are the degrees of freedom of the two populations, p is the number of parameters and F_{tab} is the theoretical value of F-distribution. In Tab. 2 we present the values for F, calculated in the equatorial coordinates (α,δ). We have normalized the values with $F_{tab}(2, N + n - 3) = 9.49122$ (where n_1 is N our number of KBOs parameter and n_2 is $n = 1593$ the number of observed KBOs (Marsden 1980)). In the table (Tab. 2) we have subtracted one from the result to make the clearer distinction that negative values represent results for which the computational and the observational distributions are statistically indistinguishable.

This test suggests that encounters with a large impact parameter b or large inclination θ are favoured (strictly speaking, the other runs are rejected on this statistical). Although this method does not makes a distinction in quality of the results, other than accepting or rejecting it, the area of parameter space that give small perturbations (blue zone) seems to be favoured. These simulations show a cold population of KBOs.

In Fig. 6 we present the fraction of KBOs that escaped the Solar System as a result of the stellar encounter. Based on these results we prefer the highly scattered regime, with a low value for b and θ (red zone). In fact only in the highly perturbed regime there is a substantial loss of mass which can reconcile the difference of two magnitude between the total mass observed and the total mass predicted by Solar System formation models (Luu & Jewitt 2002).

$b \backslash \theta$	30	60	70	80	90	100	110	120	150
225	-0.1	-0.7	-	-	-0.8	-	-	-0.9	-0.8
200	7.0	1.3	0.8	0.2	0.0	-	-	-0.7	-0.6
190	-	-	1.6	0.9	0.1	-	-	-	-
180	-	-	2.0	1.3	0.8	-	-	-	-
175	4.7	2.3	1.3	0.3	0.4	-	-	-0.6	0.0
170	-	-	-	-	0.5	0.7	-0.4	-	-
160	-	-	-	-	-0.5	0.1	-0.2	-	-
150	2.3	1.1	-	-	-0.1	0.1	-0.1	-0.3	0.1
140	-	-	-	-	-0.5	0.0	0.5	-	-

Table 2. Values of the F indicator obtained with different parameters b (listed in the left column) and θ (in the upper row) for the model A.

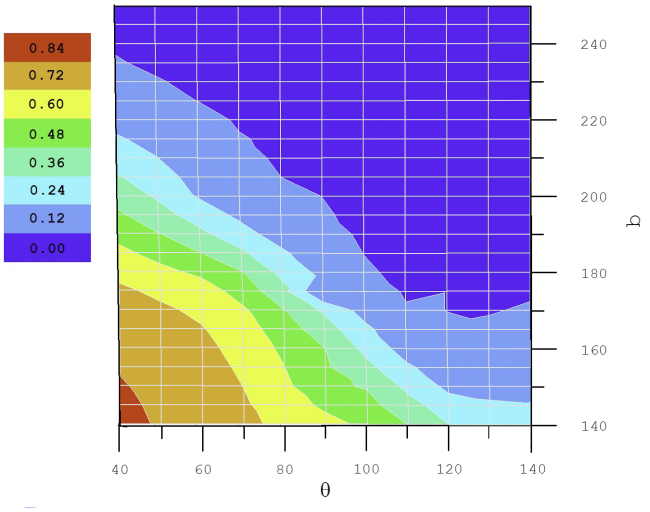


Figure 6. The 2-D surface distribution of the fraction of the KBO escaped after the gravitational encounter for the model A, at $t = 10^4$ yr, in function of the parameters b and θ. In the color map is reported for each color the mean percentage of escaper for that zone in the parameter space.

These contradicting results let us to perform a second series of simulations in which we adopted a wider range of semi-major axis, this we called model B.

3.2 Model B

In model B we adopted a wider radial extension of the KBO, 42 AU to 90 AU with a total mass of $M = 30\,M_\oplus$. The mass and encounter parameters of the incoming star are presented in Tab. 1. The success of model A in reproducing the observed parameters for the KBO led us to limit our parameter search this more extended distribution to $b = [200; 237.5]$ and $\theta = [60^\circ; 150^\circ]$. The results of the Hotelling test are presented in Tab. 3.

In Fig. 7 we present the distributions for eccentricity and inclination for $b = 200$ AU and $\theta = 90^\circ$. We determine it as the best model which gives a much better match with the observed inclinations; with value ranging from roughly 0° up to 40° in the classical regime and up to 30° in the scattered regime whereas the eccentricities of the scattered population and the hot population in the classical region are consistent with the observational data. With these parame-

$b \backslash \theta$	60	75	90	105	120	135	150
237.5	-0.6	-0.8	-0.8	-0.9	-0.8	-0.4	-0.7
225	-0.2	-0.8	-0.6	-0.7	-0.9	-0.2	-0.7
212.5	-0.3	-0.5	-0.7	-0.7	-0.8	-0.9	-0.4
200	0.1	-0.3	-0.7	-0.8	-0.5	-0.9	-0.4

Table 3. Values of the F indicator for various values of the parameters b (left column) and θ (upper row) for the model B.

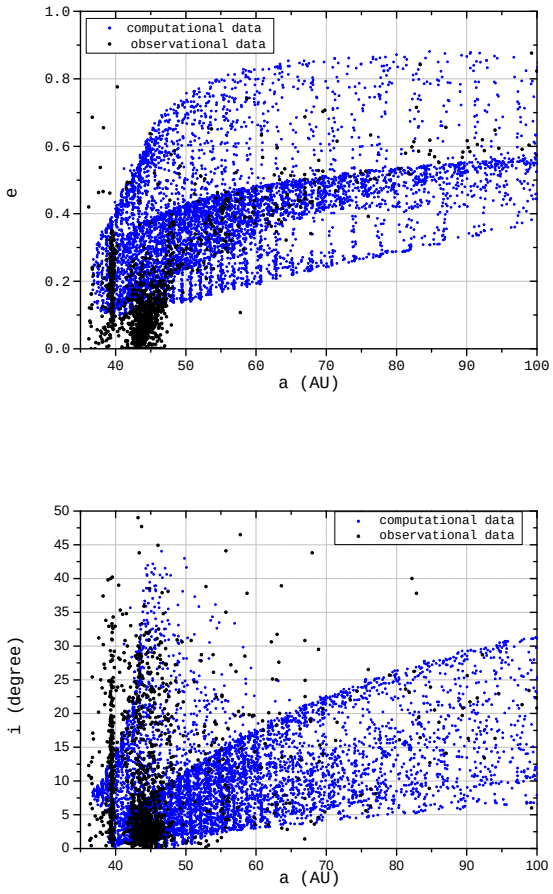


Figure 7. Comparison between the observe parameters and the result of model B directly after the scattering (at $T = 10^4$ yr) of an encounter with $b = 200AU$, $\theta = 90°$. The top panel gives the eccentricity vs. the semi-major axis, the lower panel is for the inclination.

ters the initial KB lost $\sim 13\%$ of its mass in the encounter, which is quite small compared to the predictions (Luu & Jewitt 2002).

The parameters for this particular encounter has trouble reproducing the cold population; in fact, the minimum value of the eccentricities in the classical regime 0.1. For this reason we started a series of simulations in which we study the long-term secular evolution of the KB, on which we report in § 3.3.

For comparison we highlighted, in Fig. 8 the eccentricities after the encounter for model A and model B for one particular encounter. For the range where the initial conditions of model A and B overlap, the post-encounter distributions in eccentricity and inclination also overlap. This supports the earlier argument that inter-KBO dynamics is not important during the encounter.

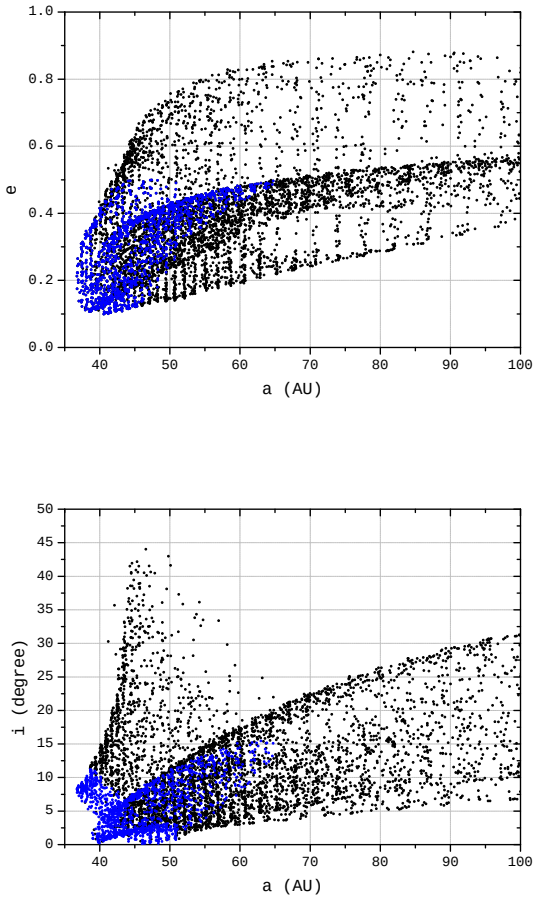


Figure 8. Distribution of eccentricities (top panel) and inclinations (bottom panel) of model A (blue) with model B (black) directly after the encounter (at $T = 10^4$ yr) with parameters $b = 200$ AU and $\theta = 90°$. This comparison is to demonstrate that model A is indeed a subset of model B, but with a higher resolution at the short-period KBOs.

3.3 Long term evolution

The main result for model A and B has been that an encounter in the early history of the Solar System can reproduce the hot KB population as well as the majority of the scattered population, but the currently observed cold population and part of the resonant populations are absent after the encounter. We will now investigate if these missing populations can be regrown by the long-term evolution of the KB.

We adopt model A with a $1\,M_\odot$ encountering star with an impact parameter $b = 200$ AU and inclination $\theta = 90°$ for this follow-up study. Ideally, we should have taken the best model B, but because the missing populations are reachable with the limited range in semi-major axes in model A, we decided that the benefit of the higher local resolution of

N	$m\ (M_\oplus)$	*relaxing of the eccentricities*
8181	3.7×10^{-3}	*yes*
8181	3.7×10^{-4}	*no*
8181	3.7×10^{-5}	*no*
4085	3.7×10^{-3}	*yes*
65525	3.7×10^{-3}	*yes*
65525	3.7×10^{-4}	*no*
65525	3.7×10^{-5}	*no*

Table 4. Entries are: the number of KBOs, N; the mass of the single KBO, m, in units of earth mass. The evolution of the first four simulations (top-down in the rows) was carried up to 0.5 Myr, while the last three were followed up to 0.1 Myr.

this model outweights the more extended width of model B. We restart the simulation at 10^4 yr after the encounter. For convenience we removed the encountering star, because it would cause numerical problems if we allowed it to continue to move further away from the Solar System, whereas it would no longer perturb the KB. Simulations were continued up to about 0.5 Myr.

In Fig. 9 we present the evolution of the eccentricities and semi-major at four moments in time. This illustrates the effect of the secular evolution of the KBOs, due to their self gravity and the influence of the planets. Whereas the encounter with the star has completely removes the cold population, the subsequent long-term evolution within the KB regrows this population. During the secular evolution the high eccentricity orbits between 37 *AU* and 46 *AU* cools and the orbital eccentricities decay. In this model we use $N = 8181$ with a total mass of 30 $M_{\rm Earth}$, which is quite massive for the KBO, each object then has a mass of $3.7 \times 10^{-3}\ M_\oplus$. In Tab. 4 we present the results of several simulations, using initial conditions from model A, up to 0.5 Myr with range of m and N. Only those simulations in which KBOs have a mass of $\sim 3.7 \times 10^{-3}\,M_{\rm Earth}$ repopulate the cold KBO.

To test the relative importance of interactions between KBOs, we rerun several of these simulations in which we turn this interaction off. These simulations did not show the cooling of the KB populations, and the eccentricities remained too high compared to the observations. We conclude that the mutual interaction among the KBOs drive the secular evolution to repopulate the cold KB population after a stellar encounter.

After establishing the initial conditions which we considered to produce the observed KB, we run one more simulations, with $N = 16,373$ and a total mass of $30\,M_{\rm Earth}$ (35% of the KBOs have a mass identical to Pluto, while the others have only one-fifth of this mass). The incoming $1\,M_\odot$ star has approaches the Sun with impact parameter $b = 200$ AU and inclination $\theta = 90°$. We continue this simulation for 0.9 Myr.

In Fig. 10 we present the energy conservation and the total number of escapers in function of time. The distribution of the eccentricities at 0.9 Myr after the encounter is shown in Fig.11.

4 CONCLUSIONS

We investigated the effect of an encounter between a passing star on the morphology of the Kuiper belt, and its subsequent long-term evolution. Using the current morphology of

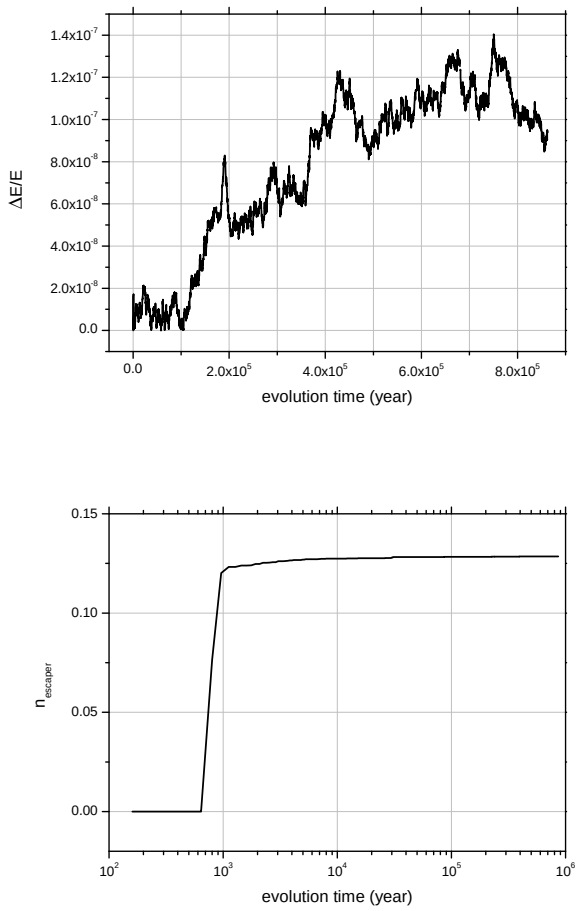


Figure 10. The relative error in the energy ($|\Delta E/E|$) (top panel) and the fraction of escapers (bottom panel) as functions of time for a $1\,M_\odot$ encounter with $b = 200$ AU and $\theta = 90°$.

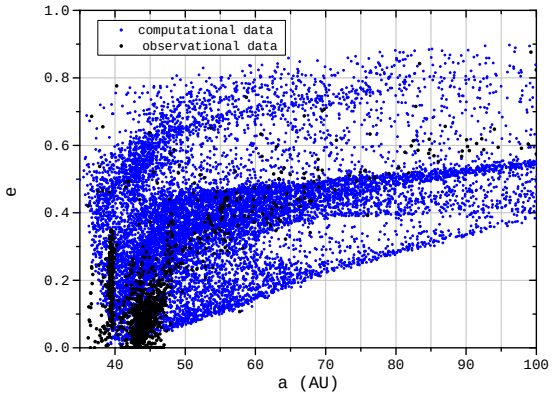


Figure 11. The eccentricities of the model B with encounter parameters $b = 200AU$ and $\theta = 90°$ at $0.9Myr$. The black dots are the observed data from the MPC (Marsden 1980) and the blue ones are the simulated data using our best model.

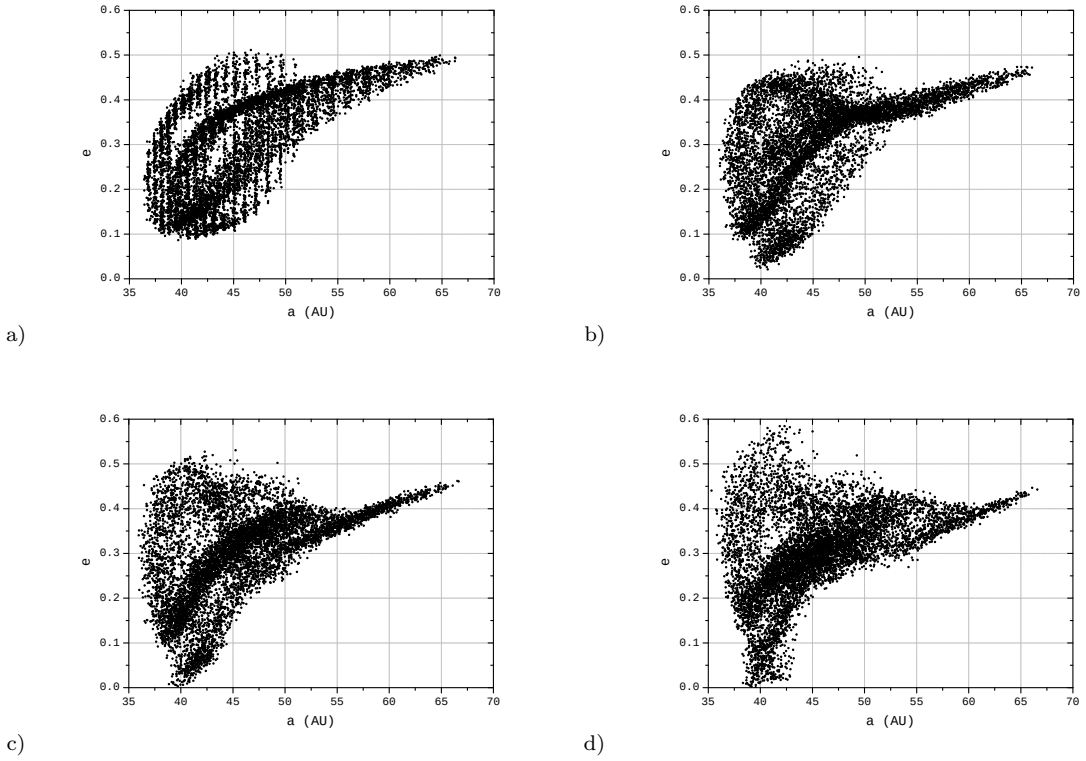


Figure 9. Time evolution of the distribution of KBOs (model A) due to the internal dynamical relaxation. The encountering star was $1\,M_\odot$, with impact parameter $b = 200$ AU and inclination $\theta = 90°$. The snapshots were taken at a) 10^4 yr, b) 1.6×10^5 yr, c) 3.2×10^5 yr and frame d at 0.5×10^6 yr.

the KB we constrained the parameter of the incoming star. The orbit of the encountering star, the planets and those of the KBOs were integrated directly, as was the subsequent evolution of the internal dynamics of the KB and planets. The initial conditions for the Solar System ware taken from Ito & Tanikawa (2002), and the Kuiper belt objects were distributed in a flat disk between 42 and 90 *AU* in the plane of the Ecliptic, and with a power law density distribution with exponent -2. The total mass of Kuiper belt ranged between 1 and 30 $M_\oplus$, and the mass of the incoming star was chosen to be $0.5\,M_\odot$ 1.0 and $2.0\,M_\odot$.

We compared the morphology of the KB directly after the encounter with the passing star, and after a secular evolution of up to 0.9 Myr. The best results, directly after the encounter, are obtained when the incoming star approached the ecliptic plane with an impact parameter of 170-220 AU and an inclination above the Ecliptic of 60° to 120°. The lower (best) values of both b and θ are for the $0.5\,M_\odot$, encountering star whereas the upper values correspond to the $2.0\,M_\odot$ intruder. During the encounter about 13% of the Kuiper belt is lost from the Solar System. We summarize these results in Tab. 5. Although possibly somewhat naive, in Fig. 12 we present the impact parameter and the angle θ of the incoming star as a function of its mass.

The morphology of the hot population of the KB are well represented directly after the encounter. This population is characterized by high inclined orbits and relatively high eccentricities. The cold population, around ~ 40 AU and with eccentricities $\lesssim 0.1$ is almost completely absent directly after the encounter. This mismatch in the morphology can be resolved by taking the secular evolution of the Kuiper belt into account. However, we were only able to reproduce this cold population, while maintaining the hot population when the Kuiper belt contained a rather large population of objects with a mass comparable to Pluto. Although, due to the limited number of objects in our simulations, it is hard to constrain either the total mass in this population of the number, we argue that a population of Pluto-mass objects are needed to drive the secular evolution of the KB to repopulate the cold population. In that case the cold population is reinstated within a million years.

A more sophisticated investigation of the long-term (many Gyr) evolution of the KB, with a proper population including the full mass-function would be hard to achieve at the moment. Although such a study could find that a smaller population of relatively massive KBOs are sufficient to repopulate the cold population (Melita et al. 2005). We therefore argue that 35% of massive KBOs is probably refers to an upper limit rather than a lower limit.

While the secular evolution repopulated the cold population, it egalized the further KB causing the depletion of the resonance population, which was initiated by the passing star. This loss of the resonant population can be caused by the insufficient sampling of the KB in our simulations. Alternatively the early migration of the planets is driving the repopulation of the resonant families (Kobayashi et al. 2005). Such planetary reordering would be a natural consequence of the Nice model (Levison et al. 2008). But at

M	0.5	1.0	2.0
b	170	200	220
v_∞	3	3	3
θ	60	90	120

Table 5. The optimal encounter parameters (b and θ) obtained for a star with mass M (in solar masses) approaching with velocity at infinity of 3 km/s the Solar System (model B). The units of b and θ are those adopted in this paper.

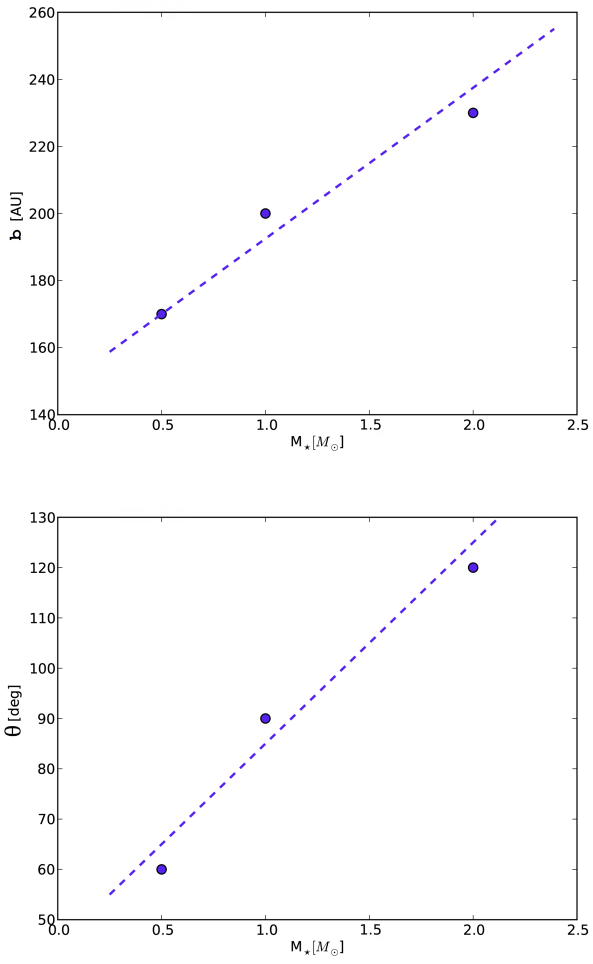


Figure 12. The impact parameter b (top) and inclination θ (bottom) as a function of the mass of the incoming star for our most favorite model (see Tab. 5). The dashed line gives a fit to the tree points to indicate the trend, which follows $b = 170 + 45(M - 0.5)$ for the impact parameter and $\theta = 65 + 40(M_\star - 0.5)$ for the inclination.

this stage we can neither rule out the mischievous effects of long-term numerical integration.

We did not study possible correlations among inclination and other properties, such as the size distribution of the KBOs and the number of KBO binaries. For instance, the KBO color correlation is still an open problem. However, the sampling in our model and the time-scale over which it was run are too limited to carry out such studies.

5 ACKNOWLEDGMENTS

D. Punzo thanks for the hospitality of Leiden Observatory (University of Leiden). This work was made possibly with financial contributions from the Dept. of Physics (Sapienza, University of Rome), Leiden Observatory the Netherlands Research Council NWO (grants #643.200.503, #639.073.803 and #614.061.608), by the Netherlands Research School for Astronomy (NOVA), and by the HPC-EUROPA2 project (project number: 1249) with the support of the European Commission - Capacities Area - Research Infrastructures. Part of the computations were carried out on the Little Green Machine at Leiden University and on the Lisa cluster at SURFSara in Amsterdam and by the computers owned by the ASTRO research group (Dep. of Physics, Sapienza, Univ. of Roma). We thank M. Spera for his help in porting the code to various architectures.

REFERENCES

Aarseth S. J., 2003, Gravitational N-Body Simulations

Bédorf J., Portegies Zwart S., 2012, European Physical Journal Special Topics, 210, 201

Berczik P., Nitadori K., Zhong S., Spurzem R., Hamada T., Wang X., Berentzen I., Veles A., Ge W., 2011, in International conference on High Performance Computing, Kyiv, Ukraine, October 8-10, 2011., p. 8-18 High performance massively parallel direct N-body simulations on large GPU clusters.. pp 8–18

Berczik P., Spurzem R., Wang L., 2013, in Third International Conference "High Performance Computing", HPC-UA 2013, p. 52-59 Up to 700k GPU cores, Kepler, and the Exascale future for simulations of star clusters around black holes.. pp 52–59

Bernstein G. M., Trilling D. E., Allen R. L., Brown M. E., Holman M., Malhotra R., 2004, Astronomical Journal, 128, 1364

Brown M. E., 2001, Astronomical Journal, 121, 2804

Brucker M. J., Grundy W. M., Stansberry J. A., Spencer J. R., Sheppard S. S., Chiang E. I., Buie M. W., 2009, Icarus, 201, 284

Capuzzo-Dolcetta R., Mastrobuono-Battisti A., Maschietti D., 2011, New Astronomy, 16, 284

Capuzzo-Dolcetta R., Spera M., 2013, Computer Physics Communications, 184, 2528

Capuzzo-Dolcetta R., Spera M., Punzo D., 2013, Journal of Computational Physics, 236, 580

Doressoundiram A., Boehnhardt H., Tegler S. C., Trujillo C., 2008, Color Properties and Trends of the Transneptunian Objects. pp 91–104

Fraser W. C., Kavelaars J. J., 2009, Astronomical Journal, 137, 72

Gomes R. S., 2003, Icarus, 161, 404

Holman M. J., 1995, in Kinoshita H., Nakai H., eds, 27th Symposium on Celestial Mechanics, The Distribution of Mass in the Kuiper Belt. p. 116

Hotelling H., 1931, Annals of Mathematical Statistics, 2, 360

Ida S., Larwood J., Burkert A., 2000, The Astrophysical Journal, 528, 351

Ito T., Tanikawa K., 2002, Monthly Notices of the Royal Astronomical Society, 336, 483

Jewitt D., Luu J., 1993, Nature, 362, 730
Kenyon S. J., Luu J. X., 1999, Astronomical Journal, 118, 1101
Kobayashi H., Ida S., 2001, Icarus, 153, 416
Kobayashi H., Ida S., Tanaka H., 2005, Icarus, 177, 246
Levison H. F., Morbidelli A., Van Laerhoven C., Gomes R., Tsiganis K., 2008, Icarus, 196, 258
Levison H. F., Stern S. A., 2001, Astronomical Journal, 121, 1730
Luu J. X., Jewitt D. C., 2002, Astronomy and Astrophysics, 40, 63
Malhotra R., 1993, Nature, 365, 819
Malhotra R., 1995, Astronomical Journal, 110, 420
Malmberg D., Davies M. B., Heggie D. C., 2011, Monthly Notices of the Royal Astronomical Society, 411, 859
Marsden B. G., 1980, Celestial Mechanics, 22, 63
Melita M. D., Larwood J. D., Williams I. P., 2005, Icarus, 173, 559
Nitadori K., Makino J., 2008, New Astronomy, 13, 498
Noll K. S., Grundy W. M., Stephens D. C., Levison H. F., Kern S. D., 2008, Icarus, 194, 758
Nyland L., Harris M., Prins J., , 2007, Fast N-Body Simulation with CUDA
Pelupessy F. I., Jänes J., Portegies Zwart S., 2012, New Astronomy, 17, 711
Pelupessy F. I., van Elteren A., de Vries N., McMillan S. L. W., Drost N., Portegies Zwart S. F., 2013, Astronomy and Astrophysics, 557, A84
Portegies Zwart S., Boekholt T., 2014, ArXiv e-prints
Portegies Zwart S., McMillan S., Harfst S., Groen D., Fujii M., Nualláin B. Ó., Glebbeek E., Heggie D., Lombardi J., Hut P., Angelou V., Banerjee S., Belkus H., Fragos T., Fregeau J., Gaburov E., Izzard R., 2009, New Astronomy, 14, 369
Portegies Zwart S., McMillan S. L. W., van Elteren E., Pelupessy I., de Vries N., 2013, Computer Physics Communications, 183, 456
Portegies Zwart S. F., 2009, The Astrophysical Journal, 696, L13
Portegies Zwart S. F., Belleman R. G., Geldof P. M., 2007, New Astronomy, 12, 641
Press W. H., Teukolsky S. A., Vetterling W. T., Flannery B. P., 2002, Numerical recipes in C++ : the art of scientific computing
Volk K., Malhotra R., 2011, The Astrophysical Journal, 736, 11